

Shot-Noise Signatures of 0.7 Structure and Spin in a Quantum Point Contact

L. DiCarlo*, Y. Zhang*, D. T. McClure*, D. J. Reilly, C. M. Marcus
Department of Physics, Harvard University, Cambridge, Massachusetts 02138, USA

L. N. Pfeiffer, K. W. West
Bell Laboratories, Lucent Technologies, Murray Hill, NJ 07974, USA
 (Dated: February 6, 2008)

We report simultaneous measurement of shot noise and dc transport in a quantum point contact as a function of source-drain bias, gate voltage, and in-plane magnetic field. Shot noise at zero field exhibits an asymmetry related to the 0.7 structure in conductance. The asymmetry in noise evolves smoothly into the symmetric signature of spin-resolved electron transmission at high field. Comparison to a phenomenological model with density-dependent level splitting yields good quantitative agreement.

Shot noise, the temporal fluctuation of current resulting from the quantization of charge, is sensitive to quantum statistics, scattering and many-body effects [1, 2]. Pioneering measurements [3, 4, 5] of shot noise in quantum point contacts (QPCs) observed the predicted [6] suppression of shot noise below the Poisson value due to Fermi statistics. In regimes where many-body effects are strong, shot noise measurements have been exploited to directly observe quasiparticle charge in strongly correlated systems [7, 8, 9] as well as to study coupled localized states in mesoscopic tunnel junctions [10] and cotunneling in nanotube-based quantum dots [11].

Paralleling these developments, a large literature has emerged concerning the surprising appearance of an additional plateau in transport through a QPC at zero magnetic field, termed 0.7 structure. Experiment [12, 13, 14] and theory [15, 16] suggest that 0.7 structure is a many-body spin effect. Its underlying microscopic origin, however, remains an outstanding problem in mesoscopic physics. This persistently unresolved issue is remarkable given the simplicity of the device.

In this Letter, we report simultaneous measurements of the shot noise at 2 MHz and dc transport in a QPC, exploring the noise signature of the 0.7 structure and its evolution with in-plane magnetic field B_{\parallel} . A suppression of the noise relative to that predicted by theory for spin-degenerate transport [6] is observed near $0.7 \times 2e^2/h$ at $B_{\parallel} = 0$, in agreement with results from Roche *et al.* [14] obtained at kHz frequencies. This suppression evolves smoothly with increasing B_{\parallel} into the signature of spin-resolved transmission. We find quantitative agreement between noise data and a phenomenological model for a density-dependent level splitting [16], with model parameters extracted solely from conductance.

Measurements are performed on a gate-defined QPC fabricated on the surface of a GaAs/Al_{0.3}Ga_{0.7}As heterostructure grown by molecular beam epitaxy (see mi-

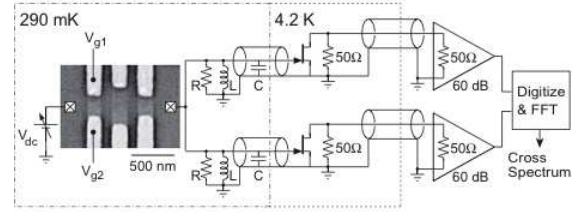


FIG. 1: Equivalent circuit near 2 MHz of the noise detection system measuring QPC noise by cross-correlation on two amplification channels [17]. The scanning electron micrograph shows a device of identical design to the one measured. The QPC is formed by negative voltages V_{g1} and V_{g2} applied on two facing electrostatic gates. All other gates on the device are grounded.

crograph in Fig. 1). The two-dimensional electron gas 190 nm below the surface has a density of $1.7 \times 10^{11} \text{ cm}^{-2}$ and mobility $5.6 \times 10^6 \text{ cm}^2/\text{Vs}$. All data reported here were taken at 290 mK, the base temperature of a ^3He cryostat.

The differential conductance $g = dI/dV_{sd}$ (where I is the current and V_{sd} is the source-drain bias) is measured by lock-in technique with an applied $25 \mu\text{V}_{\text{rms}}$ excitation at 430 Hz [17]. The resistance R_s in series with the QPC is subtracted at every applied B_{\parallel} (see Fig. 2(a)) [18].

The QPC is first characterized at zero and finite B_{\parallel} using dc conductance measurements. Figure 2(a) shows linear-response conductance $g_0 = g(V_{sd} \sim 0)$ as a function of gate voltage V_{g2} , for $B_{\parallel} = 0$ to 7.5 T in steps of 0.5 T. The QPC shows the characteristic quantization of conductance in units of $2e^2/h$ at $B_{\parallel} = 0$, and the appearance of spin-resolved plateaus at multiples of $0.5 \times 2e^2/h$ at $B_{\parallel} = 7.5$ T. Additionally, at $B_{\parallel} = 0$, a shoulder-like 0.7 structure is evident, which evolves smoothly into the $0.5 \times 2e^2/h$ spin-resolved plateau at high B_{\parallel} .

Figures 2(b) and 2(c) show g as a function of V_{sd} for evenly spaced V_{g2} settings at $B_{\parallel} = 0$ and 7.5 T, respectively. In this representation, linear-response plateaus in Fig. 2(a) appear as accumulated traces around $V_{sd} = 0$ at multiples of $2e^2/h$ for $B_{\parallel} = 0$, and at multiples of $0.5 \times 2e^2/h$ for $B_{\parallel} = 7.5$ T. At finite V_{sd} , additional

*These authors contributed equally to this work.

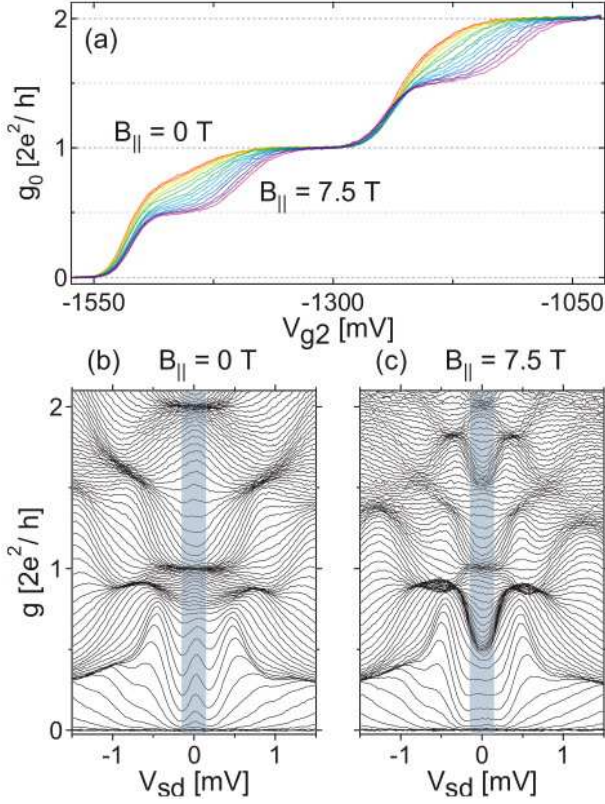


FIG. 2: (color) (a) Linear conductance g_0 as a function of V_{g2} ($V_{g1} = -3.2$ V), for $B_{||}$ ranging from 0 (red) to 7.5 T (purple) in steps of 0.5 T. The series resistance R_s ranging from 430 Ω at $B_{||} = 0$ to 730 Ω at $B_{||} = 7.5$ T has been subtracted to align the plateaus at multiples of $2e^2/h$. (b,c) Nonlinear differential conductance g as a function of V_{sd} , at $B_{||} = 0$ (b) and 7.5 T (c), with V_{g2} intervals of 7.5 and 5 mV, respectively. Shaded regions indicate the bias range used for the noise measurements presented in Figs. 3(b) and 4.

plateaus occur when a sub-band edge lies between the source and drain chemical potentials [19]. The features near $0.8 \times 2e^2/h$ ($V_{sd} \approx \pm 750$ μ V) at $B_{||} = 0$ cannot be explained in the context of a single-particle picture [12, 15]. These features are related to the 0.7 structure around $V_{sd} = 0$ and resemble the spin-resolved finite bias plateaus at $\sim 0.8 \times 2e^2/h$ for $B_{||} = 7.5$ T [12].

Turning now to noise measurements, we consider the QPC noise in excess of thermal noise $4k_B T_e g(V_{sd})$. When $1/f$ and telegraph noise as well as bias dependent heating are negligible (as shown to be the case in these data) the excess noise is dominated by noise arising from the partitioning of electrons at the QPC, which we denote as partition noise, $S_I^P(V_{sd}) = S_I(V_{sd}) - 4k_B T_e g(V_{sd})$, where S_I is the total QPC current noise spectral density. Note that S_I^P is noise in excess of $4k_B T_e g(V_{sd})$ rather than $4k_B T_e g(0)$ as considered in Refs. [3, 14].

We measure S_I^P near 2 MHz using the cross-correlation technique shown schematically in Fig. 1 to suppress amplifier voltage noise [4, 17]. Two parallel channels amplify the voltage fluctuations across a resistor-inductor-

capacitor resonator that performs current-to-voltage conversion. Each channel consists of a transconductance stage using a high electron mobility transistor (HEMT) cooled to 4.2 K, followed by 50 Ω amplification at room temperature. The amplified noise signals from both channels are sampled simultaneously by a digitizer, and their cross-spectral density calculated by fast-Fourier-transform.

The cross-spectral density is maximal at resonance, with a value

$$X_R^0 = G_X^2 \left(S_I^P \left(\frac{R_{\text{eff}}}{1 + gR_s} \right)^2 + 4k_B T_e R_{\text{eff}} \right), \quad (1)$$

where G_X is the geometric mean of the voltage gain of the amplification channels, T_e is the electron temperature and R_{eff} is the effective resistance (at 2 MHz) between the HEMT gates and ground. R_{eff} is measured from the half-power bandwidth of the cross-spectral density [17]. S_I^P is extracted from simultaneous measurements of X_R^0 , g and R_{eff} following calibration of G_X and T_e using thermal noise. At $V_{sd} = 0$, where S_I^P vanishes, $X_R^0 = G_X^2 \cdot 4k_B T_e R_{\text{eff}}$. At elevated temperatures (3 to 5 K), where electrons are well thermalized to a calibrated thermometer, a measurement of X_R^0 as a function of R_{eff} (tuned through V_{g2}) allows a calibration of $G_X = 790$ V/V. This gain is then used to determine from similar measurements the base electron temperature $T_e = 290$ mK.

Figure 3 shows $S_I^P(V_{sd})$ at $B_{||} = 0$ and fixed V_{g2} for V_{sd} between -150 μ V and $+150$ μ V (blue regions in Figs. 2(b) and 2(c)). With an integration time of 60 s at each bias point, the resolution in S_I^P is 1.4×10^{-29} A²/Hz, equivalent to full shot noise $2eI$ of $I \sim 40$ pA. Open markers superimposed on the linear conductance trace in Fig. 3(a) indicate V_{g2} settings for which corresponding noise data are shown in Fig. 3(b). S_I^P vanishes with the QPC pinched off ($g(V_{sd}) = 0$), or on linear conductance plateaus, which shows that bias-dependent electron heating is not significant [4]. In contrast, for $g \approx 0.5$ and $1.5 \times 2e^2/h$, S_I^P grows with $|V_{sd}|$ and shows a transition from quadratic to linear dependence [3, 4, 5], demonstrating the absence of noise from resistance fluctuations.

Solid curves superimposed on the $S_I^P(V_{sd})$ data in Fig. 3(b) are fits to the form

$$S_I^P(V_{sd}) = 2 \frac{2e^2}{h} \mathcal{N} \left[eV_{sd} \coth \left(\frac{eV_{sd}}{2k_B T_e} \right) - 2k_B T_e \right], \quad (2)$$

with the *noise factor* \mathcal{N} as the only free fitting parameter. Note that \mathcal{N} relates S_I^P to V_{sd} , in contrast to the Fano factor, which relates S_I^P to I [1, 2]. The form of this fitting function is motivated by mesoscopic scattering theory [1, 2, 6], where transport is described by transmission coefficients $\tau_{n,\sigma}$ (n is the transverse mode index and σ denotes spin) and partition noise originates from

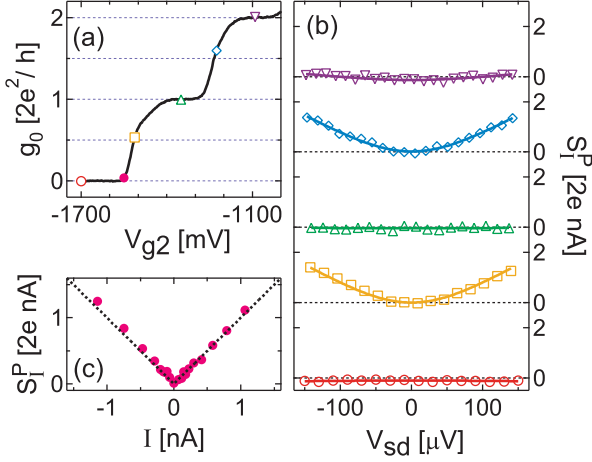


FIG. 3: (color) (a) Linear conductance g_0 as a function of V_{g2} at $B_{||} = 0$. Markers indicate V_{g2} settings for the noise measurements shown in (b) and (c). (b) Measured S_I^P as a function of V_{sd} , for conductances near 0 (red), 0.5 (orange), 1 (green), 1.5 (blue), and $2 \times 2e^2/h$ (purple). Solid lines are best-fits to Eq. (2) using \mathcal{N} as the only fitting parameter. In order of increasing conductance, best-fit \mathcal{N} values are 0.00, 0.20, 0.00, 0.19, and 0.03. (c) S_I^P as a function of dc current I with the QPC near pinch-off. The dotted line indicates full shot noise $S_I^P = 2e|I|$, comparable to results in Ref. [20].

the partial transmission of incident electrons. Within scattering theory, the full expression for S_I^P is

$$S_I^P(V_{sd}) = \frac{2e^2}{h} \int \sum_{n,\sigma} \tau_{n,\sigma}(\varepsilon) (1 - \tau_{n,\sigma}(\varepsilon)) (f_s - f_d)^2 d\varepsilon, \quad (3)$$

where $f_{s(d)}$ is the Fermi function in the source (drain) lead. Eq. (2) follows from Eq. (3) only for the case of constant transmission across the energy window of transport, with $\mathcal{N} = \frac{1}{2} \sum \tau_{n,\sigma} (1 - \tau_{n,\sigma})$. For spin-degenerate transmission, \mathcal{N} vanishes at multiples of $2e^2/h$ and reaches the maximal value 0.25 at odd multiples of $0.5 \times 2e^2/h$.

We emphasize that while Eq. (2) is motivated by scattering theory, the value of \mathcal{N} extracted from fitting with Eq. (2) simply provides a way to quantify the $S_I^P(V_{sd})$ for each V_{g2} . We have chosen the bias range $e|V_{sd}| \lesssim 5k_B T_e$ for fitting \mathcal{N} to minimize the effects of nonlinear transport while extending beyond the quadratic-to-linear crossover in noise that occurs on the scale $eV_{sd} \sim 2k_B T_e$.

The dependence of noise factor on QPC conductance at $B_{||} = 0$ is shown in Fig. 4(a), where \mathcal{N} is extracted from measured $S_I^P(V_{sd})$ at 90 values of V_{g2} . The horizontal axis, g_{avg} , is the average of the differential conductance over the bias points where noise was measured. \mathcal{N} has the shape of a dome, reaching a maximum near odd multiples of $0.5 \times 2e^2/h$ and vanishing at multiples of $2e^2/h$. The observed $\mathcal{N}(g_{avg})$ deviates from the spin-degenerate, energy-independent scattering theory in two ways. First, there is a reduction in the maximum amplitude of \mathcal{N}

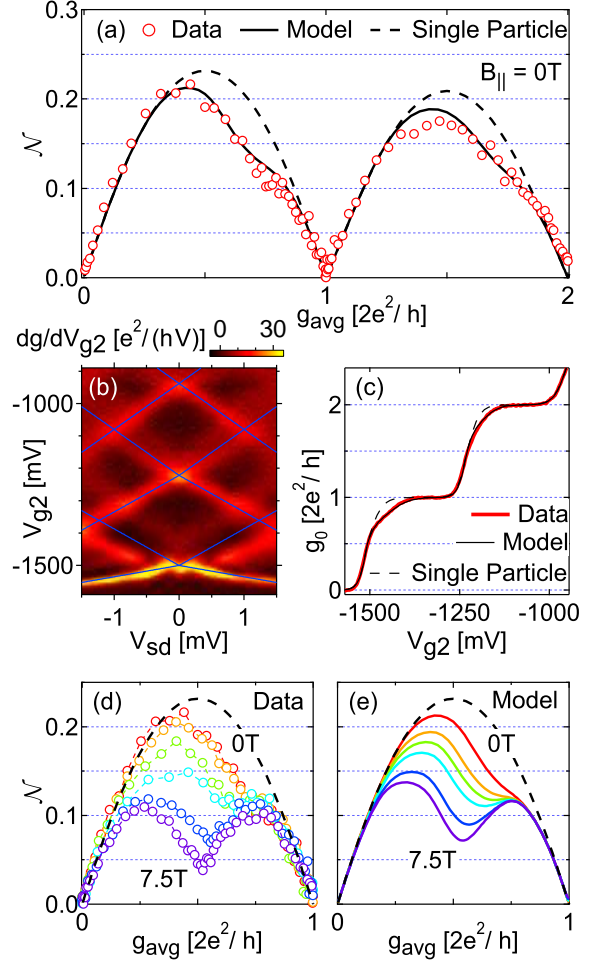


FIG. 4: (color) (a) Experimental \mathcal{N} as a function of g_{avg} at $B_{||} = 0$ (red circles) along with model curves for nonzero (solid) and zero (dashed) proportionality of splitting, γ_n (see text). (b) Transconductance dg/dV_{g2} as a function of bias voltage V_{sd} and gate voltage V_{g2} . Blue lines trace the alignment of sub-band edges with source and drain chemical potentials; their slope and intersection give the conversion from V_{g2} to energy and the energy spacing between modes, respectively [22, 23]. (c) Measured linear conductance (red) as a function of V_{g2} at $B_{||} = 0$, and linear conductance calculated with the model (black solid) with best-fit values for ω_x and γ_n . Single-particle conductance model takes $\gamma_n = 0$ (black dashed). (d) Experimental \mathcal{N} as a function of g_{avg} in the range $0 - 1 \times 2e^2/h$, at $B_{||} = 0$ T (red), 2 T (orange), 3 T (green), 4 T (cyan), 6 T (blue), and 7.5 T (purple). (e) Model curves for $\mathcal{N}(g_{avg})$ (see text). Dashed curves in (d) and (e) show the single-particle model ($\gamma_n = 0$) at zero field for comparison.

below 0.25. Second, there is an asymmetry in \mathcal{N} with respect to $0.5 \times 2e^2/h$, resulting from a noise reduction near the 0.7 feature. A similar but weaker asymmetry is observed about $1.5 \times 2e^2/h$.

The dependence of $\mathcal{N}(g_{avg})$ on $B_{||}$ is shown in Fig. 4(d). \mathcal{N} is seen to evolve smoothly from a single asymmetric dome at $B_{||} = 0$ to a symmetric double-dome at 7.5 T, the latter a signature of spin-resolved electron transmission. Notably, near $0.7 \times 2e^2/h$, \mathcal{N} appears insensitive to $B_{||}$,

in contrast to the dependence of \mathcal{N} near $0.3 \times 2e^2/h$.

We find that all features in noise data are well accounted for within a simple phenomenological model in which the twofold degeneracy of QPC mode n is lifted by a splitting $\Delta\varepsilon_{n,\sigma} = \sigma \cdot \rho_n \cdot \gamma_n$, that grows linearly with 1D density ρ_n (with proportionality γ_n) within that mode. Here, $\sigma = \pm 1/2$ and $\rho_n \propto \sum_{\sigma} \sqrt{\mu - \varepsilon_{n,\sigma}}$, (μ is the chemical potential). The lever arm converting from V_{g2} to energy (and hence ρ_n) as well transverse mode spacing are extracted from transconductance (dg/dV_{g2}) data (Fig. 4(b)). Assuming an energy-dependent transmission, $\tau_{n,\sigma}(\varepsilon) = 1/(1 + e^{2\pi(\varepsilon_{n,\sigma} - \varepsilon)/\hbar\omega_x})$, appropriate for a saddle-point potential with curvature parallel to the current described by ω_x [21], the value for ω_x is found by fitting linear conductance below $0.5 \times 2e^2/h$ (below $1.5 \times 2e^2/h$ for the second mode), and γ_n is obtained from a fit to conductance above $0.5(1.5) \times 2e^2/h$, where (within the model) the splitting is largest (see Fig. 4(c)). For the QPC studied, we find $\hbar\omega_x$ is $\sim 500(300) \mu\text{eV}$ and $\gamma_{1(2)} \sim 0.012(0.008) e^2/4\pi\epsilon_0$ for the first (second) transverse modes. Note that the splitting is two orders of magnitude smaller than the direct Coulomb energy of electrons spaced by $1/\rho_n$.

Using these parameters, model values for $S_I^P(V_{sd})$ are then calculated using the full Eq. (3), and \mathcal{N} is extracted by fitting the model $S_I^P(V_{sd})$ to Eq. (2). The resulting model values of $\mathcal{N}(g_{\text{avg}})$ at $B_{\parallel} = 0$ are shown along with the experimental data in Fig. 4(a). Also shown for comparison are the model values only accounting for energy dependent transmission but no splitting ($\gamma_n = 0$). The overall reduction of \mathcal{N} arises from a variation in transmission across the $150 \mu\text{V}$ bias window, which is comparable to $\hbar\omega_x$. Asymmetry of the model values for \mathcal{N} about 0.5 and $1.5 \times 2e^2/h$ require nonzero γ_n .

We include magnetic field in the model with corresponding simplicity by assuming a g-factor of 0.44 and adding the Zeeman splitting to the density-dependent splitting [24] maintaining the parameters obtained above. The resulting model values for \mathcal{N} are shown in Fig. 4(e), next to the corresponding experimental data (Fig. 4(d)). Experimental and model values for \mathcal{N} show comparable evolution in B_{\parallel} : the asymmetric dome at $B_{\parallel} = 0$ evolves smoothly into a double dome at 7.5 T, and for conductance $\gtrsim 0.7 \times 2e^2/h$, the curves for all magnetic fields overlap closely. Some differences are observed between data and model, particularly for $B_{\parallel} = 7.5$ T. While the experimental double-dome is symmetric with respect to the minimum at $0.5 \times 2e^2/h$, the theory curve remains slightly asymmetric with a less pronounced minimum. We find that setting the g-factor to ~ 0.6 in the model reproduces the measured symmetrical double-dome as well as the minimum value of \mathcal{N} at $0.5 \times 2e^2/h$. This observation is consistent with previous reports of an enhanced g-factor in a QPC at low-density [12].

We thank H.-A. Engel, M. Heiblum, L. Levitov and

A. Yacoby for valuable discussions, and S. K. Slater, E. Onitskansky and N. J. Craig for device fabrication. We acknowledge support from NSF-NSEC, ARO/ARDA/DTO and Harvard University.

-
- [1] Ya. M. Blanter and M. Büttiker, Phys. Rep. **336**, 1 (2000). Ya. M. Blanter, cond-mat/0511478 (2005).
 - [2] T. Martin, in *Nanophysics: Coherence and Transport*, Les Houches Session LXXXI, edited by H. Bouchiat *et al.* (Elsevier, Amsterdam, 2005), cond-mat/0501208.
 - [3] M. Reznikov *et al.*, Phys. Rev. Lett. **75**, 3340 (1995).
 - [4] A. Kumar *et al.*, Phys. Rev. Lett. **76**, 2778 (1996).
 - [5] R. C. Liu *et al.*, Nature **391**, 263 (1998).
 - [6] G. B. Lesovik, Pis'ma Zh. Eksp. Teor. Fiz. **49**, 513 (1989). [JETP. Lett. **49**, 592 (1989)]; M. Büttiker, Phys. Rev. Lett. **65**, 2901 (1990).
 - [7] R. de-Picciotto *et al.*, Nature **389**, 162 (1997); M. Reznikov *et al.*, Nature **399**, 238 (1999).
 - [8] L. Saminadayar *et al.*, Phys. Rev. Lett. **79**, 2526 (1997).
 - [9] X. Jehl *et al.*, Nature **405**, 50 (2000).
 - [10] S. S. Safonov *et al.*, Phys. Rev. Lett. **91**, 136801 (2003).
 - [11] E. Onac *et al.*, Phys. Rev. Lett. **96**, 026803 (2006).
 - [12] K. J. Thomas *et al.*, Phys. Rev. Lett. **77**, 135 (1996); A. Kristensen *et al.*, Phys. Rev. B **62**, 10950 (2000); D. J. Reilly *et al.*, Phys. Rev. B **63**, 121311(R) (2001); S. M. Cronenwett *et al.*, Phys. Rev. Lett. **88**, 226805 (2002); D. J. Reilly *et al.*, Phys. Rev. Lett. **89**, 246801 (2002);
 - [13] W. D. Oliver, Ph.D. Dissertation, Stanford University (2002).
 - [14] P. Roche *et al.*, Phys. Rev. Lett. **93**, 116602 (2004).
 - [15] C. K. Wang and K.-F. Berggren, Phys. Rev. B **54**, 14257 (1996); H. Bruus, V. V. Cheianov and K. Flensberg, Physica E **10**, 97 (2001); Y. Meir, K. Hirose and N. S. Wingreen, Phys. Rev. Lett. **89**, 196802 (2002); K. A. Matveev, Phys. Rev. Lett. **92**, 106801 (2004); A. Ramšak and J. H. Jefferson, Phys. Rev. B **71**, 161311(R) (2005).
 - [16] D. J. Reilly, Phys. Rev. B **72**, 033309 (2005).
 - [17] L. DiCarlo *et al.*, cond-mat/0406018 (2006).
 - [18] A 125 mT perpendicular magnetic field is applied throughout to minimize bias-dependent electron heating [4]. Perpendicular fields of this size do not affect the main results presented here.
 - [19] L. P. Kouwenhoven *et al.*, Phys. Rev. B **39**, 8040(R) (1989).
 - [20] Y. Chen and R. A. Webb, Phys. Rev. B **73**, 035424 (2006).
 - [21] M. Büttiker, Phys. Rev. B **41**, 7906(R) (1990).
 - [22] N. K. Patel *et al.*, Phys. Rev. B **44**, 10973(R) (1991).
 - [23] Two crossing points are observed at finite bias between the first and second modes. The model attributes this to spin splitting in the first mode. The midpoint is taken as the crossing point for the blue lines.
 - [24] In the measurement regime investigated, various ways of adding Zeeman splitting to zero-field splitting (linearly, quadrature, thermally weighted) give essentially indistinguishable results within the present model.